Colloids and Surfaces A: Physicochemical and Engineering Aspects 680 (2024) 132684

Contents lists available at ScienceDirect

Colloids and Surfaces A: Physicochemical and Engineering Aspects

journal homepage: www.elsevier.com/locate/colsurfa

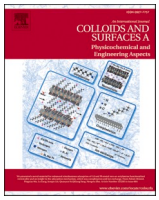

High surface area activated carbon prepared from wood-based spent mushroom substrate for supercapacitors and water treatment

Nicolas Boulanger [a], Alexandr V. Talyzin [a], Shaojun Xiong [b], Malin Hultberg [c], Alejandro Grimm [b,*]

[a] Department of Physics, Umeå University, SE-901 87 Umeå, Sweden
[b] Department of Forest Biomaterials and Technology, Swedish University of Agricultural Sciences, SE-901 83 Umeå, Sweden
[c] Department of Biosystems and Technology, Swedish University of Agricultural Sciences, SE-230 53 Alnarp, Sweden

HIGHLIGHTS

- Spent mushroom substrate (SMS) was used as precursor for production of activated carbon (AC).
- Chemical activation with KOH at 850 °C led to specific surface area of around 3000 m^2/g.
- SMS-based AC showed excellent properties for supercapacitors and water treatment.
- SMS-based supercapacitors retain 91% of their capacitance after 10,000 cycles.
- Maximum reactive orange-16 adsorption capacity according to the Liu model was 519 mg/g.

GRAPHICAL ABSTRACT

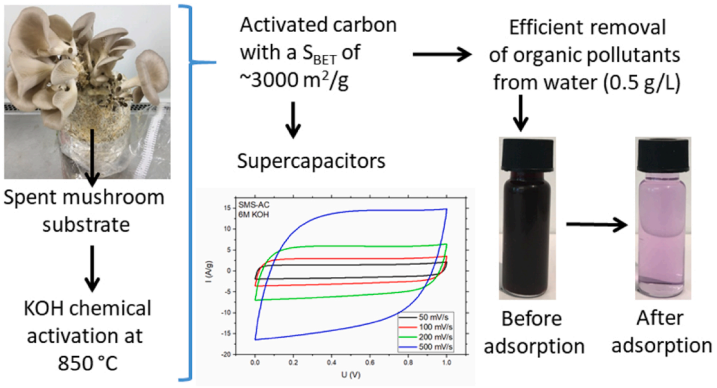

ARTICLE INFO

Keywords:
Spent mushroom substrate
Activated carbon
Supercapacitors
Adsorbents
Water treatment

ABSTRACT

Edible white-rot fungi are commonly cultivated on wood-based substrates and selectively degrade lignin to a larger extent during their growth. Spent mushroom substrate (SMS) is produced in huge amounts by the mushroom industry and today there is a lack of proven methods to valorize this kind of biomass waste, which in most cases is landfilled or used as fuel. This study demonstrates that birch wood-based SMS from the cultivation of oyster mushrooms can be converted into high-quality activated carbon (AC) with an extremely high surface area of about 3000 m^2/g. These activated carbons showed good performance when used in electrodes for supercapacitors, with energy storage parameters nearly identical to AC produced from high-quality virgin birch wood. Moreover, AC produced from SMS showed high potential as an adsorbent for cleaning reactive orange-16 azo dye from aqueous solutions as well as contaminants from synthetic effluents and from real sewage water. The kinetics of adsorption were well represented by the Avrami fractional order model and isotherms of adsorption by the Liu model. The theoretical maximum reactive orange-16 adsorption capacities were approximately 519 mg/g (SMS-based carbon) and 553 mg/g (virgin birch-based carbon). The removal of contaminants from synthetic effluents made of different dyes and inorganic compounds was around 95% and 83% depending on the

* Corresponding author.
E-mail address: Alejandro.Grimm@slu.se (A. Grimm).

https://doi.org/10.1016/j.colsurfa.2023.132684
Received 28 August 2023; Received in revised form 13 October 2023; Accepted 28 October 2023
Available online 31 October 2023

effluent composition. The removal of contaminants from raw sewage water was around 84%, and from treated sewage water was around 68%. Overall, the results showed that activated carbon prepared from waste generated during cultivation of white-rot fungi is as good as activated carbon prepared from high-quality virgin wood.

1. Introduction

Edible white-rot fungi are organisms that are cultivated using different types of substrates based on plant materials such as wood sawdust, wood logs, straw, and grasses, among others. They secrete enzymes that selectively break down lignin to a larger extent than hemicellulose and cellulose. The mushroom industry represents an important sector with a global production of around 34 million tons of edible mushrooms per year [1]. From the cultivation process, a residue known as *spent mushroom substrate* (SMS) is generated. Research has shown that wood-based SMS can be recycled, at least in part, as ingredient in mushroom substrate formulas [2–4], and biofertilizer [5]. However, approximately 3–4 tons of SMS are left behind at average mushroom farms for every ton of mushroom fruit bodies produced [6], meaning that these practices seldom resolves the disposal problem. Wood-based SMS is a good example of so-called '*difficult to reuse*' biomass waste, which is usually used as fuel to produce heat or burned on the field when there is no other alternative [7]. Other traditional disposal methods such as composting [8], is a slow process not sustainable to deal with huge amounts of different kinds of wood-based SMS. Therefore, finding alternative ways to recycle wood-based SMS by converting it into added-value products is important for resolving environmental issues of the mushroom industry.

One of the most common methods to recycle wood-based biomass waste is to convert it into biochars by thermal carbonization (pyrolysis) and to activated carbons (AC). The quality and value of activated carbons in several applications (e.g. as electrodes or as adsorbents) are mainly determined by the Specific Surface Area (SSA) and pore size distribution [9–13].

For application as adsorbent, AC is one of the most common materials used in domestic water filters. These devices are commonly used when there is a lack of reliable water sources. For example, the presence of dyes, which are commonly used in the textile industry, can cause severe damage to aquatic biosystems [14,15], and be harmful when used in agriculture or for drinking purposes. It is known that people exposed to water contaminated with dyes and/or chemicals used to produce dyes can develop cancer [16], and a wide range of health problems such as skin issues and allergies [17]. Activated carbons produced from various bio-precursors are often tested for the removal of various organic contaminants from water [18–20]. It is clear that AC with a high surface area will be more efficient when used in water treatment devices, but the pores must be sufficiently large to allow penetration of solution and accommodation of contaminant ions or molecules [13].

High surface area is also an important parameter in a second major application of AC's, that is, for preparation of electrode materials in supercapacitors [21–23]. Supercapacitors (SC) are energy storage devices based on porous electrodes that provide a surface for sorption of electrolyte ions [24]. Formation of Electric Double Layer (EDL) allows achieving energy storage millions of times higher than in standard capacitors but still lower than in batteries. The main advantages of supercapacitors are high power density, rapid charge/discharge and absence of degradation over a very large number of charge/discharge cycles. Activated carbon is the main part of industrial supercapacitors [25]. Therefore, the development of SC electrodes based on activated carbon made from diverse types of biomass wastes has gathered huge attention [26–31]. Activated carbons produced from many types of biomass waste materials were demonstrated as cheap and efficient electrode materials or adsorbents that can be produced from, e.g., pine cones [26,32–35], lignin [36], olive pits [37], waste tea-leaves [38], corn cob [39], petroleum coke [40], and sawdust [41]. Chemical activation is one of the most efficient methods used for the production of high-quality activated carbon. Among chemical activators, potassium hydroxide (KOH) is one of the most effective for obtaining large-surface-area carbons [42,43]. High surface area and good electrical conductivity are generally required properties for applications as efficient adsorbents and electrode materials in supercapacitors.

Recently we tuned KOH activation procedure to produce porous carbons with an extremely high surface area exceeding 3300 m^2/g starting from reduced graphene oxide as a precursor [9,44]. Applying the same procedure to biochars produced by thermal carbonization of pine cones, spruce cones, pine bark and wood chips was demonstrated to result in activated carbons with even higher surface area of up to approximately 3500 m^2/g [45,46]. However, all those biochars were produced using lignin-rich bio precursors. White-rot fungi are known to selectively degrade lignin meaning that SMS has higher cellulose content than the virgin wood that was used in the substrate.

In this study, we demonstrate that nearly identical high-quality AC can be prepared using both expensive virgin birch wood and inexpensive waste from mushroom production. SMS from cultivation of grey oyster mushroom was used as carbon precursor and converted into AC with a surface area of around 3000 m^2/g (BET), which demonstrated rather good performance as electrode material in supercapacitors. The SMS-based AC was also used for the removal of reactive orange-16 from water solution and contaminants from two concentrated synthetic effluents as well as real sewage water obtained from a communal treatment plant in northern Sweden, showing excellent removal performance. Therefore, this study opens new opportunities for recycling and utilization of mushroom industry waste that today represents a disposal issue.

2. Materials and methods

2.1. Carbon precursor

Spent mushroom substrate (SMS) was obtained from previous work [47], where *Pleurotus ostreatus*, known as grey oyster, was cultivated on different types of substrates. The SMS used for this work was based on birch wood (*Betula spp.*) sawdust harvested after the second flush of mushroom fruit bodies. Blocks of SMS were dried and then homogenized using a hammer mill equipped with a 3 mm screen sieve. Thereafter, was screen-sieved, and a fraction with a particle size of 1–2 mm was chosen as raw material for the preparation of activated carbon. Virgin birch wood sawdust was sieved and a fraction with the same particle size as the SMS sample was used for comparison.

2.2. Determination of major structural carbohydrates in SMS and virgin birch wood

The contents of lignin, cellulose and hemicellulose were determined using the NREL methods described elsewhere [48,49].

2.3. Production of activated carbon

The activation procedure used in this work was carried out in two steps. First, SMS or virgin birch wood samples (150 g) were pyrolysed using a tubular furnace under nitrogen atmosphere. The temperature of the sample was increased from 20 °C up to 500 °C at a rate of 5 °C/min and kept for 2 h. Afterwards, the furnace was switched off and the sample was allowed to cool to room temperature. The activation process was carried out using the chemical method with KOH [9,45,46].

Representative samples of the biochar produced in the first step were mixed with KOH in a weight ratio of 1:8. A water/ethanol (3:7 by volume) was added to the mixture using a ratio of 25 mL per gram of biochar. Afterwards, the mixture was magnetically stirred overnight and then dried in a vacuum oven to completion. The impregnated samples were annealed in a tubular muffle furnace under an argon flow. The sample was heated to 200 °C for 1 h to further dry the material before being heated for 3 h at 850 °C. The furnace was then let to cool down to room temperature. The obtained carbon was stirred overnight in 10% acetic acid in water to remove rests of the activation agent and ash. Next, the material was finally washed with water several times using a vacuum filtration setup until the pH of the wash water became neutral. The carbons were finally put to dry in a vacuum oven, resulting in activated birch wood (BW-AC) and activated spent mushroom substrate (SMS-AC). The two-step procedure, which includes pre-carbonization of bioprecursor into biochar and subsequent KOH activation is required for producing AC with a very high surface area. The process was optimized in previous research works using a set of experiments with different loading ratios (C/KOH) and temperatures of activation [9,44]. Loading carbon to KOH weight ratio of 1–8 and temperature 850 °C provided materials with the highest surface area. A precise adjustment of the KOH:carbon ratio is necessary to obtain high surface area. Using the one-step activation procedure, where the activation agent is added directly to the biomass precursor, requires less work, but lead to much smaller SSAs ($< 2000\ m^2/g$) [45,50], that are not ideal for development of devices such as supercapacitors of commercial quality.

2.4. Material characterization

The activated materials have been imaged using scanning electron microscopy (SEM) using a Carl Zeiss Merlin Field Emission Scanning Electron Microscope at an accelerating voltage of 5 kV and a current of 120 pA. The surface area of the activated materials was determined by measuring nitrogen sorption isotherms at liquid nitrogen temperature using an Autosorb iQ XR surface area and pore size analyser (Quantachrome) and values were extracted using both BET and the QSDFT equilibrium model. The measurements were done after degassing both materials at 150 °C for 24 h. Thermogravimetric analysis (TGA) was done using a TGA/DSC1 STARe device (Mettler Toledo) using nitrogen and air on a temperature ramp from 25 °C to 700 °C at a heating rate of 5 °C/min. Attenuated total reflection-Fourier-transform infrared (ATR-FTIR) spectroscopy was done using a Bruker Vertex 80 v spectrometer. Raman spectra were recorded on an inVia confocal Raman spectroscope (Renishaw) using a 514 nm laser with a 30 s acquisition time. X-ray photoelectron spectroscopy (XPS) was performed using a Kratos Axis Ultra electron spectrometer with a delay line detector. It had a 150 W monochromatic Al Kα source, a hybrid lens system resulting in an operating area of $0.3 \times 0.7\ mm^2$. A charge neutralizer was used during the measurements.

2.5. Testing in supercapacitors

Electrodes for testing energy storage parameters in supercapacitor devices have been prepared by mixing the activated material with carbon black and polytetrafluoroethylene (PTFE) in a 8:1:1 wt ratio. Ethanol was added to the mixture and the resulting paste was ground in a crucible. To prepare the pellet electrodes, different amounts of the mixture were placed in a pressure cell and compressed with a hydraulic press with a pressure of ~800 MPa (equivalent to 10 tons on a $\sim 1.2\ cm^2$ area).

Capacitors have been prepared using a Swagelok cell with two electrodes separated with a glass microfiber filter (Whatman). Two types of electrolytes have been used in the measurements: an aqueous electrolyte consisting of a 6 M potassium hydroxide (KOH) solution, and a 1 M tetraethylammonium tetrafluoroborate (TEA-BF4) solution in acetonitrile for the organic electrolyte. The cell was filled with electrolyte until saturation of the stack was reached, and then was sealed and connected to a potensiostat / galvanostat (Ivium-n-Stat). Current-voltage (CV) sweeps ranging from 0 V to 1 V (resp. 0–2.7 V) for the aqueous (resp. organic) electrolyte have been recorded at speeds of 50 mV/s, 100 mV/s, 200 mV/s and 500 mV/s. Then, electrochemical impedance spectroscopy was performed on a frequency range of 10,000 Hz down to 0.1 Hz with an amplitude of 0.1 V centred on 0 V. Next, cyclic charge discharge (CCD) curves have been recorded on a 0–1 V (resp. 0–2.7 V) for the aqueous (resp. organic) electrolyte with current densities ranging from 0.5 A/g to 100 A/g. Finally, the stability of the electrodes was determined by proceeding to 10,000 CCD charge-discharge cycles at a current density of 5 A/g.

2.6. Testing in adsorption of contaminants from water

The ability of the SMS-AC and BW-AC to remove contaminants from aqueous solutions was tested using reactive orange-16 azo dye. The effect of the AC adsorbent dosage was determined using a dye solution with a concentration of 200 mg/L (pH 6) and dosages ranging from 0.1 to 0.6 g/L. The samples were agitated at room temperature (22 °C) until equilibrium was reached. Kinetic of adsorption measurements were carried out at room temperature (22 °C) using dye solution with a concentration of 200 mg/L, an adsorbent dosage of 0.5 g/L and contact times ranging from 1 to 480 min. Adsorption isotherms were obtained by contacting dye solution with concentrations ranging from 50 to 2000 mg/L (pH 6) with 0.5 g/L of adsorbent. The samples were agitated at room temperature (22 °C) until equilibrium was reached. For all the measurements named above, the carbon adsorbent was separated from the solution by centrifugation, and the amount of dye remaining in the solution was determined by UV-Vis analysis at 494 nm. The adsorption capacity (q) and the percentage of removal were determined according to the mathematical expressions shown in supplementary materials (Eq. S1 and S2).

Representative samples of the SMS-AC and BW-AC were also tested for their capacity to remove contaminants from two synthetic effluents (Table 1) and real sewage water.

Sewage water was collected from a wastewater treatment plant in Umeå, Sweden, which treats municipal grey water coming from households. Raw water is treated using a combination of mechanical, biological and chemical treatments works to remove contaminants. Both raw and treated sewage water were used for the experiments. The treated sewage water was collected after the chemical treatment unit and was used as such. The raw sewage water was collected after the mechanical treatment where solid particles larger than 5 mm are removed. Suspended solid materials that interfered with the measurement of the concentration of contaminants in the water were removed using a paper filter before the treatment with the ACs. The pH of the raw

Table 1
Composition of the synthetic effluents.

Compounds	Concentration (mg/L)		λ_{max} (nm)
Effluent	A	B	
Acid red 18	50	50	507
Reactive orange 16	50	50	494
Reactive blue 4	50	50	595
Methylene Blue	50	50	668
Evans blue	50	50	468
Phenol Red	50	50	550
Crystal Violet	50	-	590
Methyl Red	50	-	507
Bismarck Brown	-	50	468
Methyl Orange	-	50	522
Sodium Dodecyl	25	25	-
Sodium sulfate	25	25	-
Ammonium chloride	20	25	-
Sodium acetate	20	25	-
pH	5.4	5.2	-

sewage water was 7.2 and the pH of the treated sewage water was 8.3.

The SMS-AC and the BW-AC were contacted with the synthetic effluents and sewage water using a sample dose of 0.5 g/L. The samples were agitated for 12 h using an orbital shaker at a temperature room temperature (22 °C). After that, the carbon was separated from the solution by centrifugation. The percentage of removal of contaminants after the treatment with the ACs was obtained based on the integrated area (calculated using the software Origin 2020 pro) under the UV-Vis spectra (measured using a Shimadzu 1800 UV-Vis spectrometer) before and after the treatment.

Measurements were repeated 3 times to check for experimental deviations. In all cases the deviations were around 2%.

3. Results and discussion

3.1. Structural carbohydrates and activated carbons from SMS: properties and characterization

The analysis of the contents of lignin, cellulose and hemicellulose was carried out for the SMS and virgin birch wood. It was found that the relative reduction of lignin (Klason and acid soluble) in the SMS was approximately 26%, followed by hemicellulose (13%) and cellulose (10%). This is reasonable since white-rot fungi are known to selectively degrade lignin, the reason why they are called "*delignifiers*". This degradation depends on the type of wood used in the substrate, the type of mushroom cultivated, and the cultivation time.

Activated carbons were produced in this study using SMS as a bio-precursor by a two-step procedure. The substrate was converted into biochar by thermal carbonization. The biochar was activated using KOH according to a procedure tuned in earlier studies that maximized the surface area [9,45]. The key parameters that help to produce AC with a large surface area are KOH:C proportion, homogeneous distribution of KOH around carbon grains, temperature of annealing and careful washing of the final product. A sample of virgin birch wood, i.e., the same main component of the SMS, was subjected to identical treatment to produce reference AC material.

The activated materials have been imaged using SEM shown Fig. 1. The surface of the materials shows some roughness which can be indicative of a porous structure. However, resolution of SEM is insufficient to resolve nanoporous texture of the AC revealed by analysis of nitrogen sorption isotherms. The results of the surface area and pore size distributions determined from nitrogen sorption isotherms and the QSDFT model are shown in Figs. 2 and 3. BET SSA is traditionally most often reported in the literature. However, it is argued that the cumulative SSA calculated using DFT models is likely closer to the true surface area of porous carbon materials. Therefore, both values are reported. The SSA values are similar for both studied activated carbons, with BET (cumulative) surface areas of 3160 m^2/g (2344 m^2/g) for the activated birch wood (BW-AC) and 2913 m^2/g (2169 m^2/g) for the activated spent mushroom substrate (SMS-AC). The cumulative pore volumes for both carbons are also close, with a value of 1.75 cm^3/g for the BW-AC and 1.65 cm^3/g for the SMS-AC. Pore size distribution plots show that both materials exhibit two peaks, one for micropores and a second for mesopores. Overall, the pore width is mostly below 3.5 nm, with micropores (~0.7 nm width) contributing to about 50% of the total cumulated surface area and pores with an average width of approximately 1.8 nm contributing to the other half.

While the smaller pores represent about 50% of the total cumulated surface area, they only contribute to about 25% of the total cumulated pore volume. This means that most of the space available for sorption in terms of volume is within pores with a width of around 2 nm.

Thermogravimetric data (Fig. 4) has been recorded for both the BW-AC and the SMS-AC samples in nitrogen and air by heating the sample from 25 °C to 700 °C at a speed of 5 °C/min. The TGA trace recorded under nitrogen show that the BW-AC has total weight loss of approximately 7.7% with a noticeable 2.5% weight loss step with an onset of 188 °C. Similarly, the SMS-AC sample loses 10.8% of its weight at the end of the measurement in nitrogen, with a noticeable weight loss step of 4.9% with an onset of 140 °C. This step can be attributed to the loss of remaining oxygen groups on the activated materials.

The TGA traces recorded in air help to evaluate the ash content. The part that burns in air at elevated temperatures is mostly carbon. Therefore, TGA provides information about the composition of the sample, i.e., combustible carbon part and ash content. The BW-AC sample retains 5.5% of its initial mass at the end of the measurement, with ~2.1% weight loss due to thermal reduction (onset 188 °C) and the bulk of the losses (~84.1%) around 465 °C due to oxidation of the carbon with formation of gaseous carbon oxides. Similarly, the SMS-AC retains only 7.4% of its original weight, with thermal reduction occurring at an onset of 191 °C (3.0% weight loss) and most of the weight loss at an onset of 487 °C (83.1% weight loss).

Attenuated total reflection Fourier transform infrared spectroscopy (Fig. 5a and Fig. S1 in supplementary materials) and Raman spectroscopy (Fig. 5b) of BW-AC and SMS-AC samples showed spectra typical of activated carbons developed with the activation method used here. FTIR spectra show only a rather weak signal (see Fig. S1 for full range spectra) with some bands in the 1500 – 2000 cm^{-1} typically associated with C-C and C=O stretches as it is common for nearly pure amorphous carbon. Raman spectra showed peaks from G-mode typically associated with bond stretching of sp^2 pairs and D-mode associated with lattice

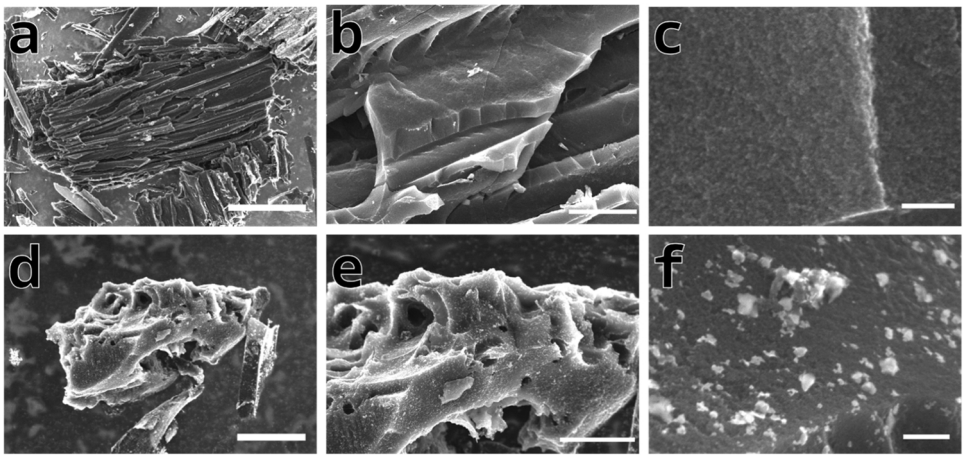

Fig. 1. Scanning electron microscopy images of a) b) and c): activated birch wood and c), d) and e): activated spent mushroom substrate. The scale bar in the pictures are a) 60 μm, b) 5 μm, c) 200 nm, d) 10 μm, e) 5 μm, and f) 200 nm.

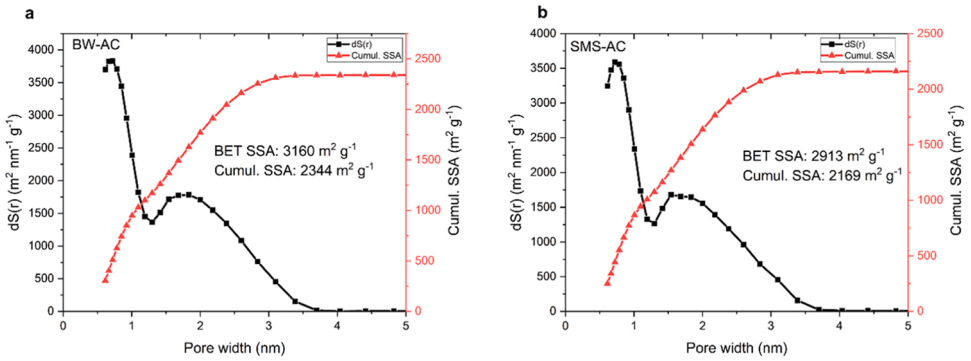

Fig. 2. Pore size distribution and cumulative pore size plots obtained using nitrogen sorption isotherms and QSDFT model for a) activated birch wood (BW-AC) and, b) activated spent mushroom substrate (SMS-AC).

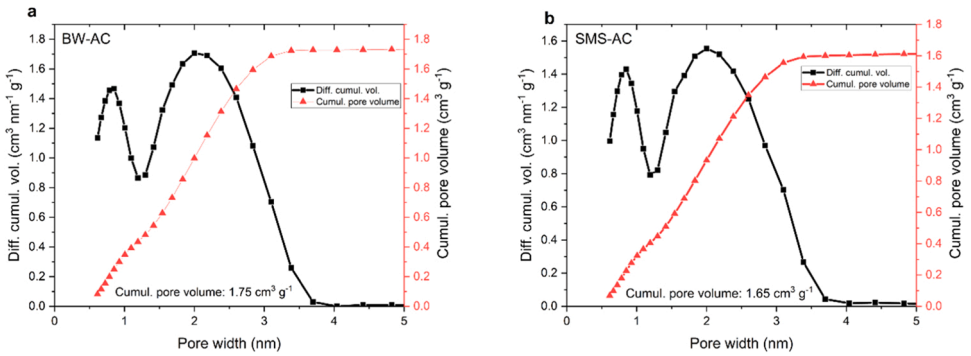

Fig. 3. Pore volume distribution and cumulative pore volume plots obtained using nitrogen sorption isotherms and QSDFT model for a) activated birch wood (BW-AC) and, b) activated spent mushroom substrate (SMS-AC).

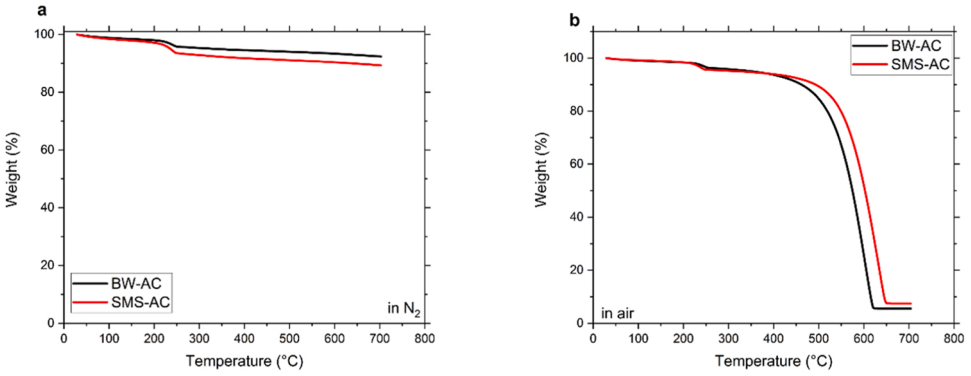

Fig. 4. TGA traces of activated birch wood (BW-AC) and activated spent mushroom substrate (SMS-AC) recorded in, a) nitrogen and b) air.

breathing mode due to disorder, with I_D/I_G values of approximately 0.95 for both samples [51].

XPS spectra (Fig. 6 and Fig. S2 and S3 in supplementary materials) recorded from BW-AC and SMS-AC confirmed that the materials are composed only of carbon and oxygen with some Al impurity (originated from the ceramic boats used for annealing). The elemental composition derived from the XPS analysis is shown in Table 2. The carbon-to-oxygen ratio (C/O) for the BW-AC sample was 8.61, and for the SMS-AC was 7.34. The trace amount of oxygen found in both samples is in agreement with the TGA data shown in Fig. 4a.

3.2. Performance of AC as electrodes in supercapacitors

Electrodes were prepared from both types of AC and tested in a standard two-electrode parallel plate setup. Pellet electrodes have been prepared by mixing the AC powder, carbon black and polytetrafluoroethylene (binder) in an 8:1:1 wt ratio. The mixture was compressed to form the pellet electrodes.

The capacitors have been first tested using a 6 M KOH aqueous electrolyte using a 0–1 V window, Fig. 7. Both carbons showed similar performance, with a capacitance recorded at 0.5 A/g of 149 F/g for BW-AC and 127 F/g for SMS-AC (~15% lower). The specific capacitance drops at higher current densities, with values dropping to 33 F/g for BW-AC (78% loss) and 35 F/g for SMS-AC (72% loss) at 80 A/g. From the Ragone plot Fig. 7d, the maximum power density and energy density were obtained for the BW-AC at 15 A/g with a power density of 5404 W/kg and an energy density of 2.69 Wh/kg. For the SMS-AC, this was achieved at 20 A/g with a power density of 6932 W/kg and an energy density of 2.04 Wh/kg.

Testing was also performed using supercapacitors with 1 M TEA-BF_4

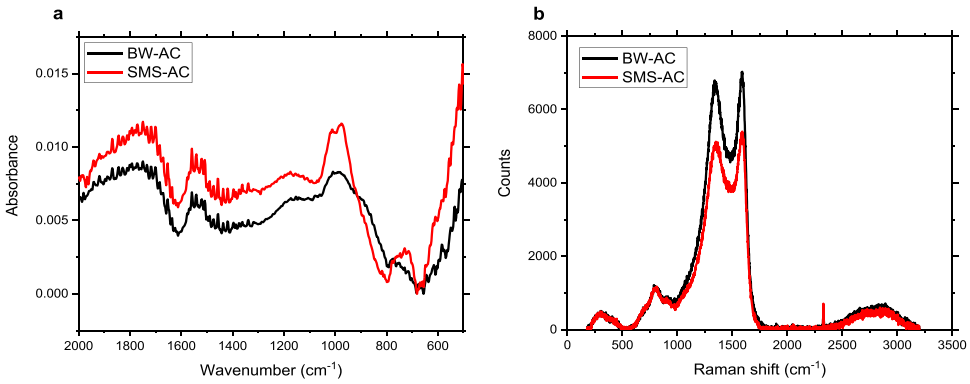

Fig. 5. a) ATR-FTIR absorbance spectra (see SI file for the figure full spectra range) and b) Raman spectra of activated birch wood (BW-AC) and activated spent mushroom substrate (SMS-AC).

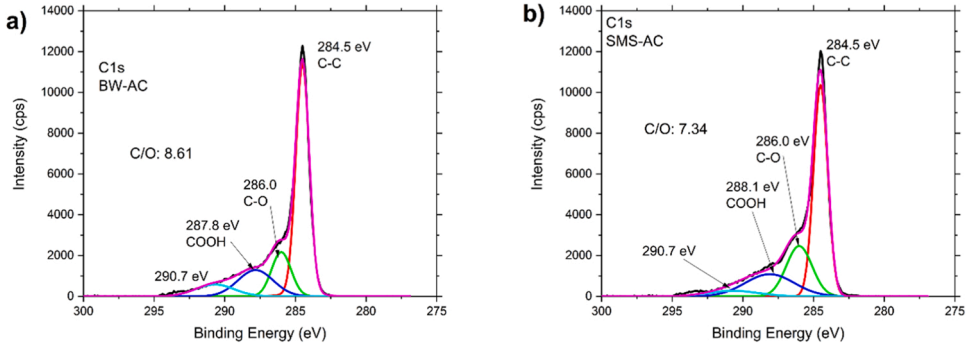

Fig. 6. C1s line of the XPS spectra of a) BW-AC, and b) SMS-AC.

Table 2
Elemental compositions of the activated carbons as measured by XPS.

		BW-AC	SMS-AC
C	C-C	51.68	43.45
	C-O	13.84	18.82
	COOH	15.01	15.72
	pi-pi	7.4	4.05
O	C═O	3.56	2.37
	C-OH	5.79	8.25
	pi-pi	1.5	1.09
N			0.6
K			4.68
Na		1.22	0.95
C/O		8.61	7.34

organic electrolyte which allows to achieve higher power/energy density using a broader voltage window of 0–2.7 V, Fig. 8. As expected, the specific capacitance is lower than the values measured in aqueous electrolyte, and the loss of capacitance when increasing the CCD current density is much stronger. The gravimetric capacitance measured from BW-AC sample is the highest at 0.5 A/g CCD current density, with a value of 106 F/g, while the SMS-AC has a specific capacitance of 87 F/g (18% lower) at the same current density. The capacitance then drops rapidly to reach a minimum value at a current density of 50 A/g for BW-AC (24 F/g, 77% loss) while SMS-AC reaches its minimum at 60 A/g with 16 F/g (82% loss). A similar drop in gravimetric capacitance was earlier found in other AC materials produced from a variety of wood-based precursors using very similar two-step pyrolysis and KOH activation procedures [46]. In this electrolyte, the BW-AC showed its best-combined performance at a current density of 10 A/g with a power density of 9164 W/kg and an energy density of 12.7 Wh/kg, while the best-combined performance of the SMS-AC was achieved at that same current density with a power density of 9873 W/kg and an energy density of 12.2 Wh/kg. Plots showing a selection of current-voltage curves recorded at different scanning speeds as well as cyclic charge discharge for both the BW-AC and SMS-AC in both the 6 M KOH and the 1 M TEA-BF_4 electrolytes are available in Supplementary Materials Fig. S4 and S5.

The electrochemical impedance spectroscopy measurements plotted in Fig. 9 show the typical behaviour of a supercapacitor, with the presence of a semicircle at high frequencies due to the device equivalent series resistance. Then a slope at ~45° can be observed which is called Warburg line and is due to the ion diffusion resistance in the material. This is more noticeable for both materials in the organic electrolyte using 1 M TEA-BF_4 compared to using the 6 M KOH aqueous electrolyte and can be explained by the smaller ion size in the aqueous electrolyte (1.33 Å for the unsolvated K^+ ion) compared to the size of the ions involved in the organic electrolyte (4.6 Å for unsolvated BF_4^-, 6.8 Å for unsolvated TEA^+) [52,53]. Finally, at lower frequencies, the slope of the Nyquist plot takes on a more vertical nature, characteristic of the capacitance dominant region.

Cycling stability measurements have been done in both organic and aqueous electrolytes by CCD at a current density of 5 A/g for 10,000 cycles, Fig. 10. The BW-AC showed lower stability, with capacitance retention of 85.6% in aqueous electrolyte and 79.6% in organic electrolyte. On the other hand, the SMS-AC showed much better stability, retaining 98.1% of its initial capacitance in aqueous electrolyte and 91.0% in organic electrolyte.

Table 3 provides a summary of BW-AC and SMS-AC material properties and their performance as electrodes in SC devices. Overall the energy storage parameters of BW-AC are somewhat better (by 10–20%) in correlation with the higher surface area and pore volume of this AC. However, SMS-AC still shows rather high energy storage values in both aqueous and organic electrolytes.

Supercapacitor with electrodes based on spent mushroom substrate

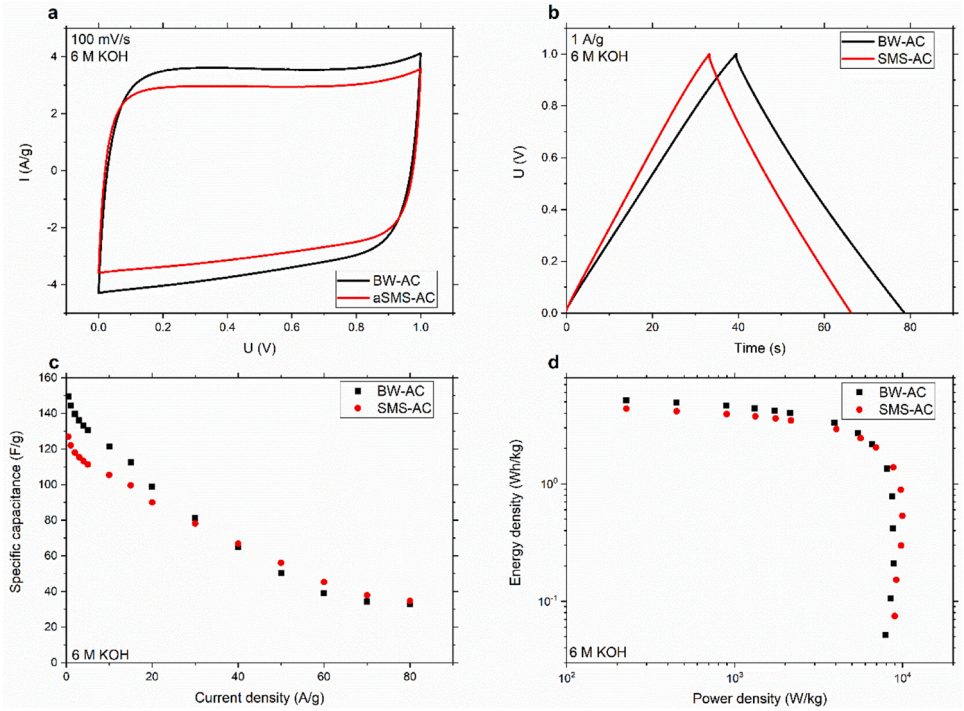

Fig. 7. Electrochemical performance of the activated birch wood and the activated spent mushroom substrate in a 6 M KOH aqueous electrolyte. a) current-voltage curves measured at 100 mV/s, b) cyclic charge-discharge curves recorded for 1 A/g, c) specific capacitance as a function of CCD current density, d) Ragone plot showing energy density and power density for different CCD current densities.

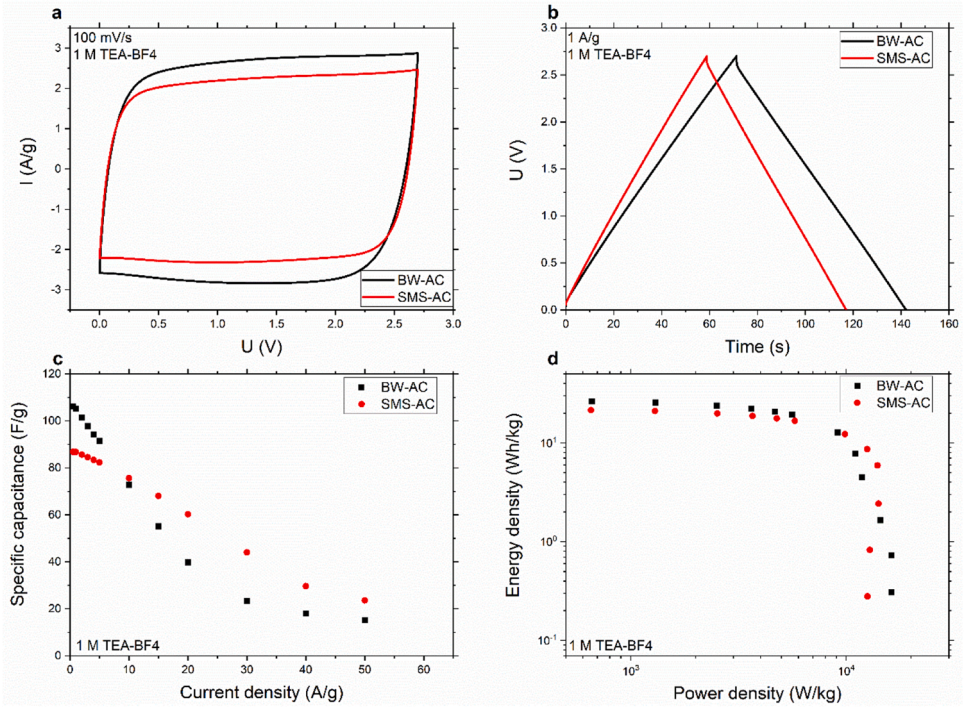

Fig. 8. Electrochemical performance of the activated birch wood and the activated spent mushroom substrate in a 1 M TEA-BF4 organic electrolyte. a) current-voltage curves measured at 100 mV/s, b) cyclic charge-discharge curves recorded for 1 A/g, c) specific capacitance as a function of CCD current density, d) Ragone plot showing energy density and power density for different CCD current densities.

demonstrated better stability over many charge-discharge cycles. In fact, the same performance as BW-AC is found in SMS-AC after 10,000 cycles. Considering that SMS is a waste with no commercial value, it is possibly beneficial to use it for the production of AC rather than high-quality virgin wood sawdust.

The performance of both AC materials in KOH and TEA-BF_4 electrolytes is in the range typically reported for high-quality activated carbons with comparable surface area in EDLC-type supercapacitors [54,55]. Clearly, the higher surface area of our AC is an advantage over carbons with lower surface area [56,57] but the overall performance of

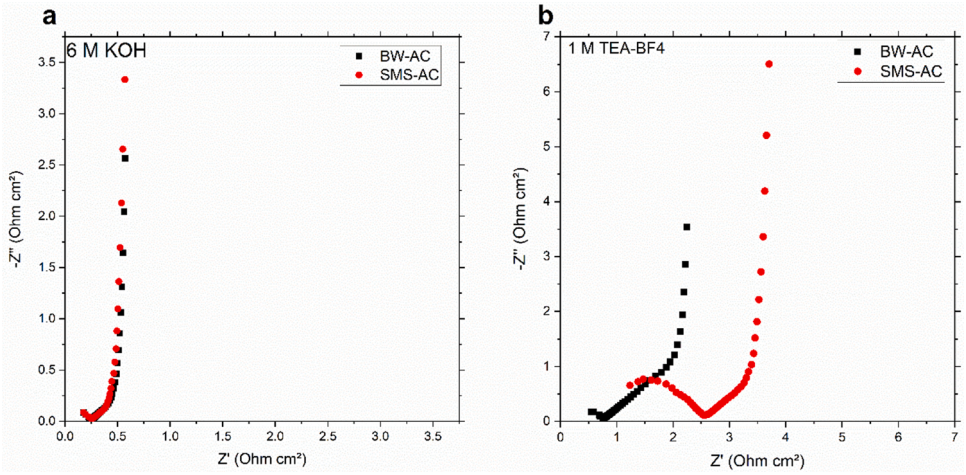

Fig. 9. Nyquist plots obtained from electrochemical impedance spectroscopy for both the activated birch wood and the activated spent mushroom substrate based electrodes in a) 6 M KOH aqueous electrolyte and b) 1 M TEA-BF4 organic electrolyte.

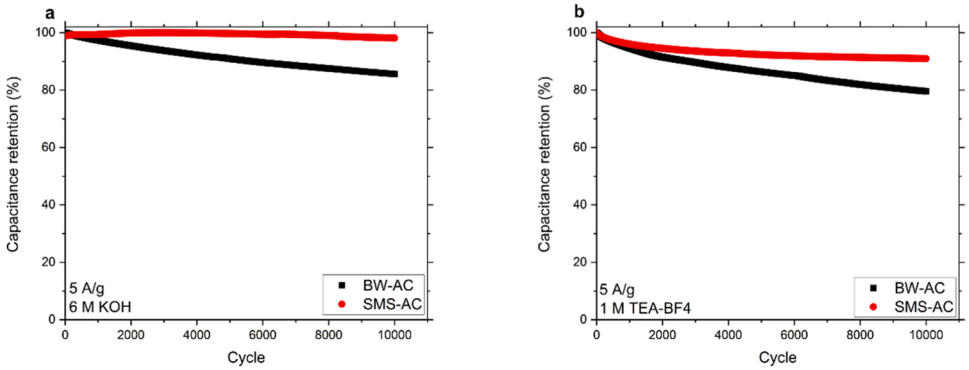

Fig. 10. Stability measurements for BW-AC and SMS-AC recorded in a) 6 M KOH aqueous electrolyte and b) 1 M TEA-BF4 organic electrolyte.

Table 3
Surface area, pore volume, capacitance and energy density for both activated carbons.

	BET Surface area [m^2/g]	DFT Surface area [m^2/g]	Total pore volume [cm^3/g]	Capacitance 1 A/g [F/g]		Energy density 10 A/g [Wh/kg]		Power density 10 A/g [W/kg]		Capacitance retention 10,000 cycles [%]	
Electrolyte				6 M KOH	1 M TEA-BF4	6 M KOH	1 M TEA-BF4	6 M KOH	1 M TEA-BF4	6 M KOH	1 M TEA-BF4
BW-AC	3160	2344	1.75	144	105	3.3	12.7	3930	9164	85.6	79.6
SMS-AC	2913	2169	1.65	122	87	2.9	12.2	4030	9873	98.1	91.0

carbon-based electrode materials depends also on several other parameters such as electrical conductivity, pore size distribution, method of electrode forming (such as binders, material loading, etc.) [9].

Interestingly, the energy storage parameters recorded here for AC produced in our study from an inexpensive waste precursor are very similar to the performance of "activated graphene" in supercapacitor devices [9,55,58]. For example, gravimetric capacitance measured in KOH electrolyte is ~150 F/g in BW-AC, which is only slightly lower compared to 166 F/g reported by Zhu et al. [58] for activated graphene. However, "activated graphene" is a lot more expensive and more difficult to prepare. The activated graphene prepared by KOH activation of reduced graphene oxide shows BET surface area, pore size distribution and performance in supercapacitors that are very similar to those reported here for AC carbons [45,59]. Using essentially cost-free biomass waste as a precursor is clearly an advantage for synthesis of high surface area carbons and practical applications in energy storage. Some values reported in the literature for supercapacitors made from biomass are listed in **Table 4** .

3.3. *Performance of AC as adsorbents*

3.3.1. *Effect of the adsorbent dosage*

Measurements of the effect of the SMS-AC and BW-AC adsorbent dosage are shown in Fig. S6 in supplementary materials. Results showed that a carbon dosage of 0.5 g/L is enough to remove almost 82% (SMS-AC) and 90% (BW-SMS) of the RO-16 dye from the aqueous solution with an initial concentration of 200 mg/L. Samples dose higher than this lead to a removal of approximately 100%, but the adsorption capacity (q) decreases drastically as the carbon dose increases. The differences in q_e between carbon dosages of 0.4 and 0.5 g/L are higher than between 0.5 and 0.6 g/L, but using 0.4 g/L leads to a percentage of removal lower than approximately 80% for both ACs. Therefore, kinetic and isotherm measurements were done using an adsorbent dosage of 0.5 g/L.

Table 4
Surface area, capacitance, power density and energy density for various activated carbons from biomass.

Material	BET Surface area [m^2/g]	Electrolyte	Specific capacitance [F/g]	Energy density [Wh/kg]	Power density [W/kg]	Reference
Olive pits	2400	1.5 M TEA-BF_4 (organic)	150			[60]
Waste soybean oil	685	0.5 M $NaPF_6$ (organic)	71	2.46	158	[56]
Sunflower seed shell	2509	30 wt% KOH (aqueous)	275	4.5	2000	[61]
Beer lees	3557	0.1 M H_2SO_4 (aqueous)	188			[62]

3.3.2. Kinetic of adsorption

Results from the kinetic measurements are shown in the supplementary materials, Fig. S7 a, c. The experimental points were fitted using the pseudo-first order, pseudo-second order second, and Avrami fractional order non-linear models according to the equations (Eq. S3-S5) given in supplementary materials. The quality of the fitting was determined using the R^2_{adj} and SD parameters obtained from the regression using equations (Eq. S9 and S10) given in supplementary materials.

The kinetic parameters obtained from the models are shown in Table 5. The pH of the RO-16 solution was measured before and after treatment with the AC to check for deviation that could affect the removal. In all cases, the pH difference was less than 2%. Fig. S8 in supplementary material show the RO-16 UV-Vis spectra before and after treatment with AC. It can be seen that the UV-Vis spectrum of the RO-16 was not affected by the adsorption process. According to the results, the kinetics of adsorption of RO-16 onto the SMS-AC and BW-AC are best represented by the Avrami fractional order model, which resulted in the highest R^2_{adj} and lowest SD. Intra-particle diffusion graphs (shown in supplementary materials Fig. S7 b, d) were obtained by potting q_t versus $t^{1/2}$, and show the presence of three stages attributed to each linear portion in the figures. The first stage that is attributed to the diffusion process of the adsorbate to the adsorbent was slightly shorter for the BW-AC probably due to the larger surface area of this carbon compared to SMS-AC. The second stage is attributed to intraparticle diffusion, and the third stage to the diffusion of the adsorbate into smaller pores, which is followed by the establishment of the equilibrium that according to the measurements was achieved at a contact time of approximately 180 min when using a dye solution with a concentration of 200 mg/L.

3.3.3. Isotherms of adsorption

Measurements were carried out using RO-16 solutions with concentrations between 50 and 2000 mg/L (pH 6) and an AC sample dose of 0.5 g/L. The experimental points were fitted using the Langmuir, Freundlich and Liu non-linear models. The mathematical expressions of these models are given in supplementary material, Eq. S6-S8. The fitting quality of each model was judged using the same methodology as described above for kinetic models. These measurements give insights into the mechanisms of adsorption as well as the theoretical maximum adsorption capacity of the activated carbons. The results from the isotherm measurements for the SMS-AC and BW-AC are shown in Fig. S9 supplementary materials, and the parameters obtained from each model are shown in Table 6. The pH of the solution before and after adsorption was measured to check for deviation that may affect the results. In all cases, the deviations in the pH were found to be less than 2%, which can be considered as an acceptable experimental error.

According to the results, the Liu model gave the highest R^2_{adj} and lowest SD. This model is a combination of the Langmuir and Freundlich models. The Liu model predicts that the active sites on an adsorbent do not have the same energy. This means that some active sites will be more preferred by the adsorbate molecules than others. However, all active sites will eventually become saturated with adsorbate molecules, unlike in the Freundlich isotherm model [63]. The theoretical maximum RO-16 adsorption capacity according to the Liu model was approximately 519 mg/g for SMS-AC and 553 mg/g for BW-AC. In Table S1, supplementary materials, is shown the maximum RO-16 adsorption capacity obtained using various types of biomass-based adsorbents. It can be seen that the adsorption capacities obtained with BW-AC and SMS-AC are slightly lower when compared to the values obtained by, e.g., Abdulhameed et al. who used crosslinked chitosan-tripolyphosphate/TiO_2 nanocomposite with a surface of 2.75 m^2/g and obtained a q_{max} of 618.7 mg/g [64]. The high sorption of RO-16 was assigned in this study to the influence of TiO_2 particles increasing sorption by a factor of 9. In absence of TiO_2 the sorption of RO-16 by SMS-AC and BW-AC is significantly higher. High sorption in absence of measurable surface area is likely a sign of chemisorption mechanism rather than physisorption typical for activated carbons. Moreover, the sorption of RO-16 is likely affected by relatively large size of the molecule relative to mostly microporous AC. Therefore, direct correlation between surface area and adsorption performance should not be expected.

The activated carbons developed here can, of course, be additionally modified by adding various nanoparticles or by chemical functionalization to improve sorption properties. It is important that AC were produced using inexpensive biomass waste from the mushroom industry, the production process is simple, and they can be used for both bio-based supercapacitors and water filters, which give some advantages compared to other products.

Table 5
Kinetic model parameters for adsorption of RO-16 onto the ACs.

	SMS-AC	BW-AC
Kinetic models		
Pseudo-first-order		
q_e (mg/g)	319.6	351.6
k_1 (1/min)	0.026	0.045
R^2_{adj}	0.987	0.982
SD (mg/g)	12.68	11.83
Pseudo-second-order		
q_e (mg/g)	363.5	385.9
k_2 (g/mg min)	8.974 E-5	1.627 E-4
R^2_{adj}	0.992	0.973
SD (mg/g)	10.33	20.57
Avrami fractional order		
q_e (mg/g)	330.5	350.1
k_a (g/mg min)	0.024	0.046
n	0.772	1.081
R^2_{adj}	0.995	0.992
SD (mg/g)	7.938	11.18

Table 6
Isotherm model parameters for adsorption of RO-16 onto the ACs.

Isotherm models	SMS-AC	BW-AC
Langmuir		
q_{max} (mg/g)	459.3	512.3
K_L (L/min)	0.093	0.131
R^2_{adj}	0.973	0.979
SD (mg/g)	28.51	27.92
Freundlich		
K_F ((mg/g) $(mg/L)_F^{-1/n}$)	186.7	216.2
n_F	7.322	7.551
R^2_{adj}	0.941	0.924
SD (mg/g)	42.32	54.36
Liu		
q_{max} (mg/g)	518.9	553.3
K_{Li} (L/mg)	0.078	0.119
N_{Li}	0.514	0.596
R^2_{adj}	0.987	0.991
SD (mg/g)	19.39	18.91

3.3.4. Removal of contaminants from synthetic effluents and sewage water

The UV-Vis spectra of both synthetic effluents and the raw and treated sewage water before and after treatment with SMS-AC and BW-AC are shown in supplementary materials Fig. S10. Note the dilution factor for effluent A and effluent B before treatment with the ACs is 5, and the dilution factor for the raw sewage water before the treatment with the ACs is 2. Samples after the treatment with the ACs were analysed as such (no dilution).

The results show that a carbon dosage of 0.5 g/L was enough to remove approximately 95% of the contaminants from effluent A and approximately 83% from effluent B. There were no remarkable differences between the SMS-AC and BW-AC. The pH of the effluents was measured before and after the treatment with the ACs to check for deviations that could affect the removal of the dyes from the solution. Deviations were found to be less than 2%. Differences in the shape of the UV-Vis spectra before and after the treatment with AC are due to molecules that are removed from the solution to a greater or lesser extent than others. This is reasonable because all the adsorbates in each effluent contain groups that can interact with the adsorbent surface and lead to a stronger or weaker attraction resulting in competition for active sites. The size of the adsorbate molecules also leads to differences in the amount of each dye remaining in the solution after treatment with the ACs.

The types and concentrations of contaminants present in the sewage water taken from the same treatment plant as the one used for this work were thoroughly analyzed in the works of Gentili & Fick [65], and Lindberg *et al.* [66]. Common contaminants found in wastewater, apart from organic matter rich in nitrogen and phosphorous, are pharmaceuticals. For the raw sewage water, around 84% of the contaminants detectable with UV-Vis were removed. The amount of contaminants that can be detected with UV-Vis in the treated sewage water collected after chemical treatment done at the plant is very low. Most of the contaminants present in the raw sewage water are removed during the biological and chemical treatments and end up in the activated sludge obtained from the processes. However, treatment with AC of this water was able to remove up to approximately 68% of the contaminants (detectable by UV-Vis) left after the treatments carried out in the wastewater treatment facility. These results demonstrate that the activated carbon produced from SMS is as effective as the one produce from virgin birch wood. The utilization of SMS to produce added-value products such as activated carbon that can be used in water treatment devices would help valorize waste that today is considered as a disposal problem.

The FTIR and XPS analyses of the ACs (Fig. 5a, Table 2, and Fig. S2 in supplementary materials) showed that the carbons developed by KOH activation have oxygen surface groups that might contribute to the removal of the organic contaminants from aqueous solutions. However, due to the large surface area of the activated carbons, the removal of contaminants from the water was achieved mainly through physical interaction between the dyes and the carbon porous structure following the pore-filling adsorption mechanism. Other mechanisms such as electrostatic, hydrogen bonding, π-π and Lewis acid-base interactions probably took place, but to a lesser extent.

3.4. Limitations of this study and recommendations

This work was carried out using spent substrate from the cultivation of grey oyster (*Pleurotus* ostreatus) mushroom collected after the second flush of fruit bodies. The degradation and relative relation between cellulose, hemicellulose and lignin in the SMS change, of course, with the type of fungi and cultivation time, i.e., the longer the cultivation time, the higher the degradation becomes. For example, mycelia of mushrooms such as shiitake (*Lentinula edodes*) or king oyster (*Pleurotus eryngii*), are known to take a longer time to grow and produce fruit bodies compared to *Pleurotus ostreatus*, and therefore, lead to SMS that is degraded to a larger extent. The development and characterization of activated carbon for supercapacitor electrodes using other types of SMS is part of future papers, but what can be said is that differences in SMS composition will probably have some effect (both positive and negative) on the results.

The results from this work could help to achieve the sustainable development goals of the United Nations related to clean water and sanitation (UNSDG-6), affordable and clean energy (UNSDG-7), responsible consumption and production (UNSDG-12), climate action (UNSDG-13), life below water (UNSDG-14).

4. Conclusions

Birch wood-based spent mushroom substrate (SMS) obtained from the cultivation of grey oyster mushrooms was used to produce high-quality activated carbon with an extremely high surface area of approximately 3000 m^2/g. Virgin birch wood (BW) was used for comparison. The activated carbons produced from SMS were used as electrode material in supercapacitors and as adsorbents for the removal of contaminants from synthetic effluents and sewage water. The specific surface area, pore size distribution and chemical composition of the activated carbon produced from SMS were very similar to those that were found in BW activated carbon. The energy storage parameters of electrodes tested in supercapacitor devices appeared to be almost the same for both activated carbons produced from BW and SMS when using a 6 M KOH and 1 M TEA-BF4 electrolytes. However, the activated SMS showed better stability, retaining 98.1% of its initial capacitance in aqueous electrolyte and 91.0% in organic electrolyte after 10,000 charge-discharge cycles. The activated carbon made from SMS was as efficient as the BW sample during the removal of reactive orange-16 as well as contaminants from concentrated synthetic effluents and sewage water. The kinetics of adsorption were well represented by the Avrami fractional order model and isotherms of adsorption by the Liu model. The theoretical maximum dye adsorption capacities were approximately 519 mg/g (SMS-based carbon) and 553 mg/g (virgin birch-based carbon). The removal of contaminants from the water was achieved mainly through physical interaction through the pore-filling mechanism. It can be concluded that low-cost waste generated in mushroom industries can be converted into activated carbons of similar quality as activated carbon produced from more expensive virgin wood precursors. The concept shown in this paper could help to reduce the environmental impact of important sectors such as the food industry.

CRediT authorship contribution statement

Funding acquisition: A.G., A.T., S.X., M.H. Conceptualization: A.G., A. T. Methodology: A.G., A. T., N. B. Investigation, visualization and data curation: A.G., A. T., N. B. Formal analysis A.G., A. T., N. B. Supervision: A.G., A. T. Writing – original draft: A.G., A. T., N. B. Writing-review and editing: all authors.

Declaration of Competing Interest

The authors declare the following financial interests/personal relationships which may be considered as potential competing interests: Alejandro Grimm reports financial support was provided by Swedish Research Council Formas.

Data Availability

Data will be made available on request.

Acknowledgements

A.G., A.T., S.X and M.H. acknowledge financial support from the Swedish Research Council Formas (grant No. 2021-00877). A. T. acknowledges funding from Energimyndigheten (No. 50620-1). The authors also acknowledge the Vibrational Spectroscopy Platform of Umeå

University and A. Shchukarev for support with the XPS measurements.

Appendix A. Supporting information

Supplementary data associated with this article can be found in the online version at doi:10.1016/j.colsurfa.2023.132684.

References

[1] FAOSTAT, Mushrooms and Truffles, ⟨http://www.fao.org/faostat/en/#data/QC⟩, (2021).
[2] D. Royse, Use of spent mushroom substrate (SMS) as an ingredient in mushroom compost formulations, Mushroom Sci. 18 (2012) 709–713.
[3] W.A. Wan Mahari, W.L. Nam, C. Sonne, W. Peng, X.Y. Phang, R.K. Liew, P.N. Y. Yek, X.Y. Lee, O.W. Wen, P.L. Show, W.-H. Chen, J.-S. Chang, S.S. Lam, Applying microwave vacuum pyrolysis to design moisture retention and pH neutralizing palm kernel shell biochar for mushroom production, Bioresour. Technol. 312 (2020).
[4] S.S. Lam, X.Y. Lee, W.L. Nam, X.Y. Phang, R.K. Liew, P.N.Y. Yek, Y.L. Ho, N.L. Ma, M.H.N.B. Rosli, Microwave vacuum pyrolysis conversion of waste mushroom substrate into biochar for use as growth medium in mushroom cultivation, J. Chem. Technol. Biotechnol. 94 (2019) 1406–1415.
[5] M.N. Owaid, I.A. Abed, S.S.S. Al-Saeedi, Applicable properties of the bio-fertilizer spent mushroom substrate in organic systems as a byproduct from the cultivation of Pleurotus spp, Inf. Process. Agric. 4 (2017) 78–82.
[6] A.D. Singh, S. Vikineswary, N. Abdullah, M. Sekaran, Enzymes from spent mushroom substrate of Pleurotus sajor-caju for the decolourisation and detoxification of textile dyes, World J. Micro Biot. 27 (2011) 535–545.
[7] J.L. Huang, J.Y. Liu, J.C. Chen, W.M. Xie, J.H. Kuo, X.W. Lu, K.L. Chang, S.T. Wen, G. Sun, H.M. Cai, M. Buyukada, F. Evrendilek, Combustion behaviors of spent mushroom substrate using TG-MS and TG-FTIR: Thermal conversion, kinetic, thermodynamic and emission analyses, Bioresour. Technol. 266 (2018) 389–397.
[8] L.Q. Meng, W.G. Li, S.M. Zhang, C.D. Wu, L.Y. Lv, Feasibility of co-composting of sewage sludge, spent mushroom substrate and wheat straw, Bioresour. Technol. 226 (2017) 39–45.
[9] A. Iakunkov, V. Skrypnychuk, A. Nordenstrom, E.A. Shilayeva, M. Korobov, M. Prodana, M. Enachescu, S.H. Larsson, A.V. Talyzin, Activated graphene as a material for supercapacitor electrodes: effects of surface area, pore size distribution and hydrophilicity, Phys. Chem. Chem. Phys. 21 (2019) 17901–17912.
[10] R. Mysyk, E. Raymundo-Pinero, F. Beguin, Saturation of subnanometer pores in an electric double-layer capacitor, Electrochem Commun. 11 (2009) 554–556.
[11] Y.H. Lu, S.L. Zhang, J.M. Yin, C.C. Bai, J.H. Zhang, Y.X. Li, Y. Yang, Z. Ge, M. Zhang, L. Wei, M.X. Ma, Y.F. Ma, Y.S. Chen, Mesoporous activated carbon materials with ultrahigh mesopore volume and effective specific surface area for high performance supercapacitors, Carbon 124 (2017) 64–71.
[12] P.C. Gao, W.Y. Tsai, B. Daffos, P.L. Taberna, C.R. Perez, Y. Gogotsi, P. Simon, F. Favier, Graphene-like carbide derived carbon for high-power supercapacitors, Nano Energy 12 (2015) 197–206.
[13] A. Bhatnagar, W. Hogland, M. Marques, M. Sillanpaa, An overview of the modification methods of activated carbon for its water treatment applications, Chem. Eng. J. 219 (2013) 499–511.
[14] T. Setiadi, Y. Andriani, M. Erlania, Treatment of textile wastewater by a combination of anaerobic and aerobic processes: a denim processing plant case, Proc. Southeast Asian Water Environ. 1 (2006).
[15] M.M. Hassan, C.M. Carr, A critical review on recent advancements of the removal of reactive dyes from dyehouse effluent by ion-exchange adsorbents, Chemosphere 209 (2018) 201–219.
[16] G. Choudhary, Human health perspectives on environmental exposure to benzidine: a review, Chemosphere 32 (1996) 267–291.
[17] R. Kishor, D. Purchase, G.D. Saratale, R.G. Saratale, L.F.R. Ferreira, M. Bilal, R. Chandra, R.N. Bharagava, Ecotoxicological and health concerns of persistent coloring pollutants of textile industry wastewater and treatment approaches for environmental safety, J. Environ. Chem. Eng. 9 (2021).
[18] Y.Ld.O. Salomón, J. Georgin, D.S.P. Franco, M.S. Netto, D.G.A. Piccilli, E.L. Foletto, L.F.S. Oliveira, G.L. Dotto, High-performance removal of 2,4-dichlorophenoxy-acetic acid herbicide in water using activated carbon derived from Queen palm fruit endocarp (Syagrus romanzoffiana), J. Environ. Chem. Eng. 9 (2021).
[19] A.F.M. Streit, G.C. Collazzo, S.P. Druzian, R.S. Verdi, E.L. Foletto, L.F.S. Oliveira, G. L. Dotto, Adsorption of ibuprofen, ketoprofen, and paracetamol onto activated carbon prepared from effluent treatment plant sludge of the beverage industry, Chemosphere 262 (2021).
[20] J.S. Lazarotto, K. da Boit Martinello, J. Georgin, D.S.P. Franco, M.S. Netto, D.G. A. Piccilli, L.F.O. Silva, E.C. Lima, G.L. Dotto, Preparation of activated carbon from the residues of the mushroom (Agaricus bisporus) production chain for the adsorption of the 2,4-dichlorophenoxyacetic herbicide, J. Environ. Chem. Eng. 9 (2021).
[21] A. Gonzalez, E. Goikolea, J.A. Barrena, R. Mysyk, Review on supercapacitors: technologies and materials, Renew. Sust. Energ. Rev. 58 (2016) 1189–1206.
[22] D.Y. Qu, H. Shi, Studies of activated carbons used in double-layer capacitors, J. Power Sources 74 (1998) 99–107.
[23] G.P. Wang, L. Zhang, J.J. Zhang, A review of electrode materials for electrochemical supercapacitors, Chem. Soc. Rev. 41 (2012) 797–828.
[24] X.F. Lu, G.R. Li, Y.X. Tong, A review of negative electrode materials for electrochemical supercapacitors, Sci. China Technol. Sc. 58 (2015) 1799–1808.
[25] V.V.N. Obreja, A. Dinescu, A.C. Obreja, Activated carbon based electrodes in commercial supercapacitors and their performance, Int Rev. Electr. Eng. -I 5 (2010) 272–281a.
[26] A. Bello, N. Manyala, F. Barzegar, A.A. Khaleed, D.Y. Momodu, J.K. Dangbegnon, Renewable pine cone biomass derived carbon materials for supercapacitor application, Rsc Adv. 6 (2016) 1800–1809.
[27] M. Genovese, K. Lian, Polyoxometalate modified pine cone biochar carbon for supercapacitor electrodes, J. Mater. Chem. A 5 (2017) 3939–3947.
[28] M. Rajesh, R. Manikandan, S. Park, B.C. Kim, W.J. Cho, K.H. Yu, C.J. Raj, Pinecone biomass-derived activated carbon: the potential electrode material for the development of symmetric and asymmetric supercapacitors, Int J. Energ. Res 44 (2020) 8591–8605.
[29] K. Karthikeyan, S. Amaresh, S.N. Lee, X.L. Sun, V. Aravindan, Y.G. Lee, Y.S. Lee, Construction of high-energy-density supercapacitors from pine-cone-derived high-surface-area carbons, Chemsuschem 7 (2014) 1435–1442.
[30] N. Manyala, A. Bello, F. Barzegar, A.A. Khaleed, D.Y. Momodu, J.K. Dangbegnon, Coniferous pine biomass: a novel insight into sustainable carbon materials for supercapacitors electrode, Mater. Chem. Phys. 182 (2016) 139–147.
[31] M.Y. Bhat, N. Yadav, S.A. Hashmi, Pinecone-derived porous activated carbon for high performance all-solid-state electrical double layer capacitors fabricated with flexible gel polymer electrolytes, Electro Acta 304 (2019) 94–108.
[32] K.M. Li, S.C. Tian, J.G. Jiang, J.M. Wang, X.J. Chen, F. Yan, Pine cone shell-based activated carbon used for CO_2 adsorption, J. Mater. Chem. A 4 (2016) 5223–5234.
[33] G. Duman, Y. Onalt, C. Okutucu, S. Onenc, J. Yanik, Production of activated carbon from pine cone and evaluation of its physical, chemical, and adsorption properties, Energ. Fuel 23 (2009) 2197–2204.
[34] S. Dawood, T.K. Sen, C. Phan, Synthesis and characterisation of novel-activated carbon from waste biomass pine cone and its application in the removal of congo red dye from aqueous solution by adsorption, Water Air Soil Poll. 225 (2014).
[35] M. Momcilovic, M. Purenovic, A. Bojic, A. Zarubica, M. Randelovic, Removal of lead(II) ions from aqueous solutions by adsorption onto pine cone activated carbon, Desalination 276 (2011) 53–59.
[36] A.M. Navarro-Suarez, J. Carretero-Gonzalez, V. Roddatis, E. Goikolea, J. Segalini, E. Redondo, T. Rojo, R. Mysyk, Nanoporous carbons from natural lignin: study of structural-textural properties and application to organic-based supercapacitors, Rsc Adv. 4 (2014) 48336–48343.
[37] E. Redondo, J. Carretero-Gonzalez, E. Goikolea, J. Segalini, R. Mysyk, Effect of pore texture on performance of activated carbon supercapacitor electrodes derived from olive pits, Electro Acta 160 (2015) 178–184.
[38] C. Peng, X.B. Yan, R.T. Wang, J.W. Lang, Y.J. Ou, Q.J. Xue, Promising activated carbons derived from waste tea-leaves and their application in high performance supercapacitors electrodes, Electro Acta 87 (2013) 401–408.
[39] W.T. Tsai, C.Y. Chang, S.L. Lee, Preparation and characterization of activated carbons from corn cob, Carbon 35 (1997) 1198–1200.
[40] T. Otowa, R. Tanibata, M. Itoh, Production and adsorption characteristics of MAXSORB: high-surface-area active carbon, Gas. Sep. Purif. 7 (1993) 241–245.
[41] B.H. Hameed, A.L. Ahmad, K.N.A. Latiff, Adsorption of basic dye (methylene blue) onto activated carbon prepared from rattan sawdust, Dyes Pigments 75 (2007) 143–149.
[42] T. Otowa, Y. Nojima, T. Miyazaki, Development of KOH activated high surface area carbon and its application to drinking water purification, Carbon 35 (1997) 1315–1319.
[43] T. Otowa, Y. Nojima, M. Itoh, Activation mechanism, surface properties and adsorption characteristics of KOH activated high surface area carbon, Springer Int Ser Eng,, 1996, pp. 709–716.
[44] A. Klechikov, G. Mercier, T. Sharifi, I.A. Baburin, G. Seifert, A.V. Talyzin, Hydrogen storage in high surface area graphene scaffolds, Chem. Commun. 51 (2015) 15280–15283.
[45] A. Nordenstrom, N. Boulanger, A. Iakunkov, G. Li, R. Mysyk, G. Bracciale, P. Bondavalli, A.V. Talyzin, High-surface-area activated carbon from pine cones for semi-industrial spray deposition of supercapacitor electrodes, Nanoscale Adv. 4 (2022) 4689–4700.
[46] G. Li, A. Iakunkov, N. Boulanger, O.A. Lazar, M. Enachescu, A. Grimm, A. V. Talyzin, Activated carbons with extremely high surface area produced from cones, bark and wood using the same procedure, Rsc Adv. 13 (2023) 14543–14553.
[47] A. Grimm, F. Chen, G.S. dos Reis, V. Dinh, S.G. Khokarale, M. Finell, J.P. Mikkola, M. Hultberg, G.L. Dotto, S.J. Xiong, Cellulose fiber rejects as raw material for integrated production of pleurotus spp. mushrooms and activated biochar for removal of emerging pollutants from aqueous media, Acs Omega 8 (2023) 5361–5376.
[48] F. Chen, S. Xiong, J. Sundelin, C. Martín, M. Hultberg, Potential for combined production of food and biofuel: cultivation of pleurotus pulmonarius on soft- and hardwood sawdusts, J. Clean. Prod. 266 (2020).
[49] A. Sluiter, B. Hames, R. Ruiz, C. Scarlata, J. Sluiter, D. Templeton, D. Crocker, Determination of structural carbohydrates and lignin in biomass, Lab. Anal. Proced. 1617 (2008) 1–16.
[50] A. Iakunkov, A. Klechikov, J.H. Sun, T. Steenhaut, S. Hermans, Y. Filinchuk, A. Talyzin, Gravimetric tank method to evaluate material-enhanced hydrogen storage by physisorbing materials, Phys. Chem. Chem. Phys. 20 (2018) 27983–27991.
[51] A. Lazzarini, A. Piovano, R. Pellegrini, G. Leofanti, G. Agostini, S. Rudić, M. R. Chierotti, R. Gobetto, A. Battiato, G. Spoto, A. Zecchina, C. Lamberti, E. Groppo, A comprehensive approach to investigate the structural and surface properties of

activated carbons and related Pd-based catalysts, Catal. Sci. Technol. 6 (2016) 4910–4922.
[52] I.I. Misnon, R.A. Aziz, N.K.M. Zain, B. Vidhyadharan, S.G. Krishnan, R. Jose, High performance MnO2 nanoflower electrode and the relationship between solvated ion size and specific capacitance in highly conductive electrolytes, Mater. Res. Bull. 57 (2014) 221–230.
[53] G. Feng, J. Huang, B.G. Sumpter, V. Meunier, R. Qiao, Structure and dynamics of electrical double layers in organic electrolytes, Phys. Chem. Chem. Phys. 12 (2010).
[54] E. Frackowiak, F. Beguin, Carbon materials for the electrochemical storage of energy in capacitors, Carbon 39 (2001) 937–950.
[55] T. Kim, G. Jung, S. Yoo, K.S. Suh, R.S. Ruoff, Activated graphene-based carbons as supercapacitor electrodes with macro- and mesopores, Acs Nano 7 (2013) 6899–6905.
[56] R. Kumari, V. Singh, C.R. Kant, Enhanced performance of activated carbon-based supercapacitor derived from waste soybean oil with coffee ground additives, Mater. Chem. Phys. 305 (2023).
[57] M. Sevilla, R. Mokaya, Energy storage applications of activated carbons: supercapacitors and hydrogen storage, Energ. Environ. Sci. 7 (2014) 1250–1280.
[58] Y.W. Zhu, S. Murali, M.D. Stoller, K.J. Ganesh, W.W. Cai, P.J. Ferreira, A. Pirkle, R. M. Wallace, K.A. Cychosz, M. Thommes, D. Su, E.A. Stach, R.S. Ruoff, Carbon-based supercapacitors produced by activation of graphene, Science 332 (2011) 1537–1541.
[59] N. Boulanger, V. Skrypnychuk, A. Nordenstrom, G. Moreno-Fernandez, M. Granados-Moreno, D. Carriazo, R. Mysyk, G. Bracciale, P. Bondavalli, A. V. Talyzin, Spray deposition of supercapacitor electrodes using environmentally friendly aqueous activated graphene and activated carbon dispersions for industrial implementation, Chemelectrochem 8 (2021) 1349–1361.
[60] E. Redondo, J. Ségalini, J. Carretero-González, E. Goikolea, R. Mysyk, Relation between texture and high-rate capacitance of oppositely charged microporous carbons from biomass waste in acetonitrile-based supercapacitors, Electro Acta 293 (2019) 496–503.
[61] X. Li, W. Xing, S. Zhuo, J. Zhou, F. Li, S.-Z. Qiao, G.-Q. Lu, Preparation of capacitor's electrode from sunflower seed shell, Bioresour. Technol. 102 (2011) 1118–1123.
[62] S.G. Lee, K.H. Park, W.G. Shim, M.S. balathanigaimani, H. Moon, Performance of electrochemical double layer capacitors using highly porous activated carbons prepared from beer lees, J. Ind. Eng. Chem. 17 (2011) 450–454.
[63] Y. Liu, A general model for biosorption of Cd2+, Cu2+ and Zn2+ by aerobic granules, J. Biotechnol. 102 (2003) 233–239.
[64] A.S. Abdulhameed, A.-T. Mohammad, A.H. Jawad, Application of response surface methodology for enhanced synthesis of chitosan tripolyphosphate/TiO2 nanocomposite and adsorption of reactive orange 16 dye, J. Clean. Prod. 232 (2019) 43–56.
[65] F.G. Gentili, J. Fick, Algal cultivation in urban wastewater: an efficient way to reduce pharmaceutical pollutants, J. Appl. Phycol. 29 (2017) 255–262.
[66] R.H. Lindberg, S. Namazkar, S. Lage, M. Ostman, Z. Gojkovic, C. Funk, F.G. Gentili, M. Tysklind, Fate of active pharmaceutical ingredients in a northern high-rate algal pond fed with municipal wastewater, Chemosphere 271 (2021).